Preprints of the 19th World Congress
The International Federation of Automatic Control
Cape Town, South Africa. August 24-29, 2014

Accelerometer-based online reconstruction of vibrations in extremely large telescopes ⋆

Alexander Keck [*,**] **Jörg-Uwe Pott** [**] **Oliver Sawodny** [*]

[*] *Institute for System Dynamics (ISYS), University of Stuttgart, Pfaffenwaldring 9, Stuttgart 70569, Germany (E-mail: alexander.keck@isys.uni-stuttgart.de, Telephone: +49 711 685 65927)*
[**] *Max Planck Institute for Astronomy (MPIA), Königstuhl 17, Heidelberg 69117, Germany*

Abstract: Recent efforts to improve imaging quality of extremely large telescopes are based on compensating for structural vibrations with a compensation mirror canceling out the optical pathway deviations caused by vibrations of the telescope structure. To drive this mirror, the displacement of optical elements has to be reconstructed online from accelerometer measurements. The goal is to obtain high reconstruction accuracy and good disturbance rejection in spite of low-frequency drift and high-frequency noise highly deteriorating the measurements. A reconstructor based on double integration and filtering, a disturbance observer and a novel reconstruction approach based on adaptive resonators are implemented on a laboratory test setup simulating typical telescope vibrations. The true displacement is measured with a strain gauge and serves as a reference for reconstruction accuracy.

Keywords: Accelerometers; Position estimation; Vibration measurement; Telescopes; Adaptive systems; Micro and Nano Mechatronic Systems; Precision measurements; Linear systems.

1. INTRODUCTION

Extremely large telescopes are utilized for ground-based astronomical observations allowing scientists to observe distant stars, galaxies and extrasolar planets. The telescopes' imaging quality and their ability to observe faint stars at the diffraction limit is limited by two major effects distorting the light emerging from the observed area: Turbulences in earth's atmosphere distort the light's wavefronts before arrival at the telescope and vibrations of the telescope's mechanical structure distort the optical path between the telescope's primary mirror and the imaging camera.

Adaptive optical systems are used to improve the distorted image. An adaptive optical system is a specialized form of a control system, measuring the wavefront distortion and correcting it, Fig. 1.

In this classical layout, the wavefront deformation caused by the atmosphere and the distortions caused by the telescope's mechanical vibrations are measured with only one sensor, the wavefront sensor, and corrected in a single control loop utilizing two actuators for tip-tilt and wavefront correction, respectively.

From a control engineering point of view, this setup can be represented by the signal-flow diagram in Fig. 2. Wavefront sensors (WFS) are in general a combination of optics and charge-coupled-devices (CCDs). The obtained image is used in sophisticated algorithms for wavefront reconstruction, Hardy [1998] and the control effort is distributed to the two correctors.

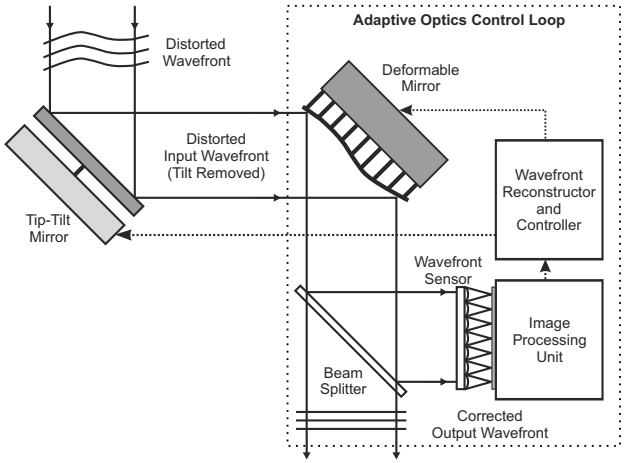

Fig. 1. Typical adaptive optics setup, adopted from Ruppel et al. [2013]

CCDs are basically arrays of photo-sensitive capacitors, integrating the accumulated light during the exposure time T. It is obvious that large exposure times on the main imaging camera as well as the similar wavefront sensor are desirable for high-contrast imaging, especially when observing faint stars. The fixed exposure time T imposes the characteristics of a digital control system with T as the sampling time on the adaptive optics compensation setup and causes limitations to its performance. The choice of sample time T limits the largest disturbance frequency that can be compensated, since the control bandwidth

⋆ This work was supported by the German Federal Ministry of Education and Research (BMBF) under grant 05A11VS1.

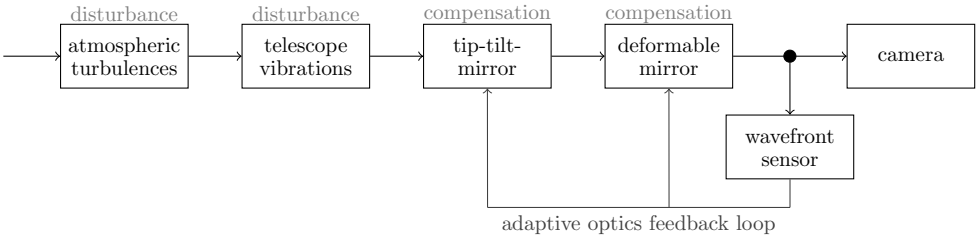

Fig. 2. Control systems representation of a typical adaptive optics system

is limited by the Nyquist-Frequency of the control loop. The largest targeted disturbance frequency thus defines the upper limit for the exposure time T.

However, this goal is opposing the goal to have large sampling times in order to obtain high imaging contrast as described previously. As a conclusion, the requirements for an adaptive optics control system considering the largest frequency that can be compensated and considering the imaging contrast, are contradictory and thus the controller performance will be far from optimal.

Telescope vibrations distort the pathlength between the telescope's mirrors and not the surface shape of the mirrors, the resulting errors are thus limited to angular displacements of the entire light beam, so-called tip-tilt errors. Experience from existing extremely large telescopes shows that the major source for high-frequency tip-tilt disturbances with $f > 5\,\mathrm{Hz}$, Böhm et al. [2013], are vibrations of the telescope's structure, while atmospheric tip-tilt disturbances are mostly of lower frequency. High-order wavefront abberations will not be caused by telescope vibrations. Modal analysis of extremely large telescopes, e.g. Böhm et al. [2013], revealed that only few resonant peaks in the modal spectrum of the telescope's mechanical structure account for the most part of optical pathway deviations.

2. PROPOSED CONTROL SYSTEM

These considerations are the foundation for the proposed new control system architecture as shown in Fig. 4. In order to allow a good compensation for disturbances from both sources, two separated control systems have to be used. The typical feedback control loop of an adaptive optics system remains unchanged in its structure and compensates for low-frequency disturbances. It can thus be operated at small sampling rates, resulting in a large sampling time T and thus in in high exposure times at the CCD-sensor.

The high-frequency disturbances caused by telescope vibrations are compensated for by the following disturbance feedforward system: The vibrations are measured using accelerometers, Kürster et al. [2010], the overall disturbance angle in the optical path is reconstructed from these measurements. The reconstructed disturbance angle is then fed to the already existing tip-tilt mirror, Fig. 1 to use this mirror to cancel out the disturbances. From a control engineering viewpoint, this setup is a disturbance feedforward system, Fig. 4. Acting as a feedforward system, the system cancels out distortions before the optical image is affected. The compensation of all high-frequency disturbances before they arrive at the feedback control loop allows to design the adaptive optics feedback loop solely for the remaining low-frequency wavefront distortions. Ultimately, the proposed control system permits observing faint stars with sufficient imaging contrasts on both the wavefront sensor and the main observational camera while disturbances caused by mechanical vibrations of the telescope structure are compensated for.

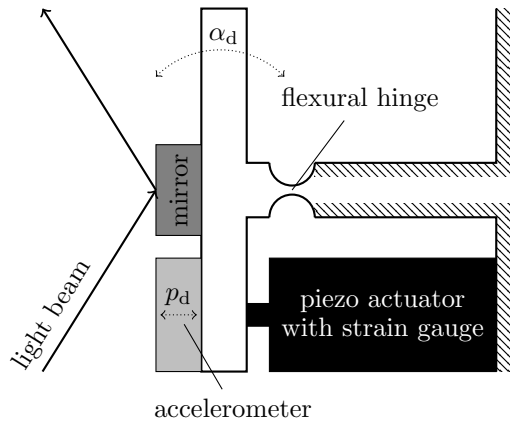

Fig. 3. Schematical drawing of the test setup

Although the application of accelerometers requires the design of a position reconstruction system, there are hardly any other types of sensors fulfilling the given requirements available. Mounting strain gauges along the telescope structure would permit the direct measurement of displacement signals rather than acceleration signals, however reconstructing the mirror displacement from the measurement of several strain gauge signals at different positions along the telescope constitutes presumably an even more difficult reconstruction problem. A direct measurement of the mirror displacement using laser vibrometers is not possible because any scattered laser light inside the telescope would corrupt astronomical observations.

This paper focuses on the reconstruction of displacement caused by disturbance vibrations based on accelerometer measurements. Obviously, a good reconstruction performance is the basic prerequisite for the feedforward compensation of vibration induced disturbances in the optical path.

The test setup is depicted in Fig. 3. A mirror within the light path is tilted to simulate the tip-tilt disturbances caused by vibration of optical elements in the telescope. A piezo actuator (*Piezosystem Jena PA 8/14 SG*) is used in this unit, the piezo's linear range of $7.6\,\mu\mathrm{m}$ is converted to an angular range of $0.3\,\mathrm{mrad} = 1\,\mathrm{arcmin}$ by a flexural hinge that permits frictionless movements for small an-

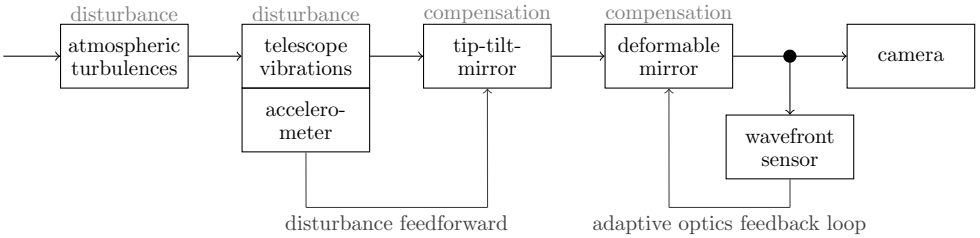

Fig. 4. Proposed control system architecture.

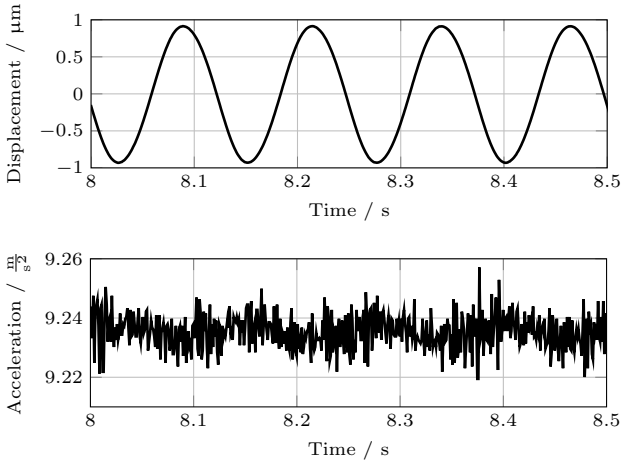

Fig. 5. Test case 8 Hz vibration: strain gauge displacement measurement p_d and accelerometer signal a

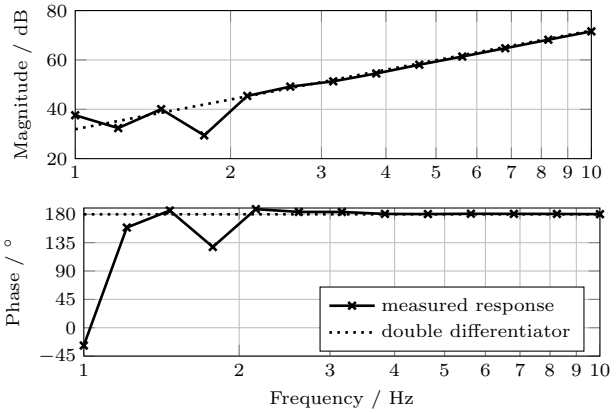

Fig. 6. Measured Frequency Response of the Accelerometer, strain gauge signal p_d to accelerometer signal a

gles, Slocum [1992]. The piezo actuator is equipped with a strain gauge to meausure the displacement with high accuracy. The angular movement of the mirror α_d can be converted to the linear displacement of the piezo p_d, thus the strain gauge measurement will be used as the reference for position reconstruction. Note that this strain gauge is only available at the laboratory setup, not at the real telescope. It provides a calibrated displacement measurement and is used to validate the accelerometer-based position reconstruction system in the laboratory, before the reconstruction system is implemented at the telescope. The piezoelectric accelerometer (*PCB Piezotronics 393B05*) is driven by this linear displacement and the accelerometer output signal is the basis for all reconstructor approaches.

Only few resonant frequencies in the range of 5–30 Hz account for the most part of optical pathway deviations, Böhm et al. [2013]. Thus, the considered test case is a sinusoidal disturbance vibration at $\omega_0 = 8\,\mathrm{Hz}$ with an amplitude of $p_{\mathrm{d,Amp}} = 0.8\,\mu\mathrm{m}$. The corresponding strain gauge and accelerometer signals are shown in Fig. 5. The accelerometer signals are highly deteriorated by noise and low-frequency drifts, even though the selected accelerometers are high-accuracy grade. A measurement of the accelerometer's frequency response (transfer function from strain gauge measurement to accelerometer measurement) was performed to further investigate the low-frequency behavior, Fig. 6. As can be seen there, the accelerometers used in the experimental setup generate low-frequency disturbance components deviating from the indicated ideal double differentiating response for $f < 4\,\mathrm{Hz}$.

3. POSITION RECONSTRUCTION

The major control engineering task in this setup is reconstructing the disturbance displacement p_d from the accelerometer measurements a, as shown in Fig. 5, in order to use this estimate $\hat{p}_\mathrm{d}$ to cancel out the disturbances with the tip-tilt correction mirror. A good reconstructor for this task has to fulfill two requirements: Double integrating behaviour at the targeted disturbance frequency ω_0 (a magnitude of $1/\omega_0^2$ and -180 ° of phase) and strong attenuation of both low-frequency drifts and high-frequency noise.

Three different reconstructor approaches will be presented and evaluated in this section: a combination of high-pass filter and double integrator, a disturbance observer and a reconstructor based on adaptive resonators.

3.1 Double Integrator and Filter

The intuitive approach to acquire a position estimate from accelerometer measurements is simply double integration. High-frequency noise is attenuated well by the double integrator, due to its -40 $\mathrm{dB/dec}$ magnitude behaviour. Constant or low-frequency offsets, on the other hand, will cause diverging behavior, due to the double integrator's unstable behaviour. This problem is usually adressed by a high-pass filter attenuating these disturbances, Godhavn [1998]. The overall transfer function of the double integrator and high-pass filter is given in (1), Godhavn [1998], with the measured acceleration signal a and the estimated position $\hat{p_\mathrm{d}}$. ω_c denotes the filter corner frequency, the damping ζ is usually chosen as $\zeta = 1/\sqrt{2}$ to place the poles on a Butterworth contour. The cut-off frequency ω_c is chosen well below the targeted disturbance frequencies ω_0

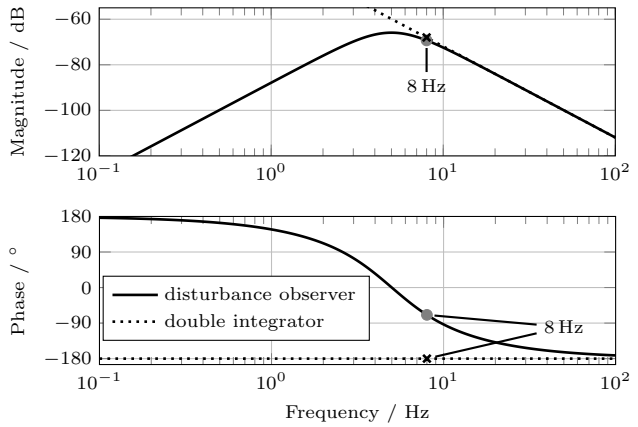

Fig. 7. Calculated Frequency Response of the double integrator with high-pass filter: Acceleration measurement a to estimated position $\hat{p}_\mathrm{d}$

but large enough to attenuate all low-frequency drifts in the measurement chain.

$$H_\mathrm{filt}(s) = \frac{\hat{p}_\mathrm{d}}{a}(s) = \frac{s^2}{\left(s^2 + 2\zeta\omega_\mathrm{c}s + \omega_\mathrm{c}^2\right)^2} \tag{1}$$

Due to two zeros at the origin, the transfer function has zero DC gain, followed by a $+40\,\mathrm{dB/dec}$ slope in the frequency band of offsets and low-frequency drifts which are thus attenuated well. This double differentiating behavior ends at the corner frequency ω_c and is followed by double integrating behavior used for the targeted disturbance frequencies ω_0 that can be placed all over this frequency range. This $-40\,\mathrm{dB/dec}$ slope at higher frequencies also ensures good noise attenuation.

A problem arises when the spectral distance between low-frequency disturbances and actual spectral components of the movement is small. The high-pass corner frequency in our setup has to be chosen as $f = 5\,\mathrm{Hz}$ to attenuate the low-frequency disturbance components, resulting in the overall reconstruction performance shown in the bode plot Fig. 7 and the experimental results in Fig. 8. As can be seen there, the magnitude at the 8 Hz test frequency is reasonably close to the desired double integrating behavior. However, the phase at 8 Hz (marked by a gray dot) is still in transition from double differentiating to double integrating behavior and is thus more than 90 ° off the desired -180 ° (marked by a black cross).

There are several approaches to supplement this reconstructor with filters that induce phase lag to lower the phase to -180 ° without changing the magnitude, similar to an all-pass filter. However, these filters are either designed to reach -180 ° at only one single frequency while deteriorating the phase behavior for all larger frequencies, or the high-frequency amplification is increased. The first class of filters cannot be applied to the considered problem because several vibration frequencies have to be targeted, Böhm et al. [2013], the second class of filters will increase noise amplification which is not desirable given the high level of measurement noise.

The reconstructor approach based on double integration and filtering attenuates low-frequency drifts and high-frequency noise well. Unfortunately, it does not work well

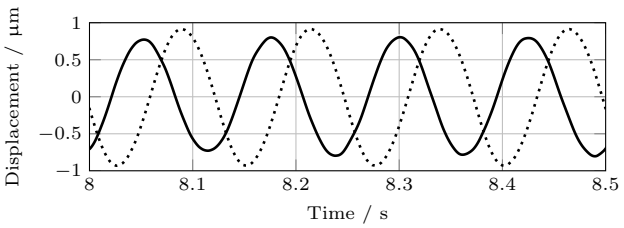

Fig. 8. Position estimated by double integration and high-pass filtering; solid: estimation $\hat{p}_\mathrm{d}$; dotted: strain gauge measurement p_d

for disturbance frequencies ω_0 close to the accelerometer's drift dynamics, as in our case, since a phase lead is induced.

3.2 Disturbance Observer

To overcome this drawback, a second approach was investigated. A common solution to the given problem is a disturbance observer based on a fictional system generating the disturbance signals, Franklin et al. [1997]. Caused by a structural resonance, the disturbance will be a sinusoidal signal with frequency ω_0, which can be regarded as the output of an autonomous system (2). The low-frequency drifts are regarded as constant for the purpose of observer design (3). Acting as an estimator for initial states, the observer will adapt to slowly varying drifts of this constant.

The differential equations (2) and (3) are converted to the state space system (4) with the state variables $\underline{x} = [p_\mathrm{d}\ \dot{p}_\mathrm{d}\ a_\mathrm{offs}]^\mathrm{T}$ The system output is the measured acceleration a including the measurement offset a_offs.

$$\ddot{p}_\mathrm{d} = -\omega_0^2\ p_\mathrm{d} \tag{2}$$

$$\dot{a}_\mathrm{offs} = 0 \tag{3}$$

$$\dot{\underline{x}} = \begin{bmatrix} 0 & 1 & 0 \\ -\omega_0^2 & 0 & 0 \\ 0 & 0 & 0 \end{bmatrix} \underline{x}$$

$$y = a = \ddot{p}_\mathrm{d} + a_\mathrm{offs} = \begin{bmatrix} -\omega_0^2 & 0 & 1 \end{bmatrix} \underline{x} \tag{4}$$

The observability matrix $\mathbf{P}$ has full rank and the system is thus observable for all $\omega_0 \neq 0$,

$$\mathbf{P} = \begin{bmatrix} -\omega_0^2 & 0 & 1 \\ 0 & -\omega_0^2 & 0 \\ \omega_0^4 & 0 & 0 \end{bmatrix} \underline{x}$$

$$\det \mathbf{P} = \omega_0^6. \tag{5}$$

A Luenberger observer was designed by Pole-Placement for this disturbance system. Since the disturbance system is an autonomous system, the observer does only require one input to the measured acceleration a to estimate the disturbance position $\hat{p}_\mathrm{d}$.

The reconstruction performance for the experiment with an 8 Hz, 0.8 µm sinusoid is depicted in Fig. 9. This reconstruction approach permits position reconstruction without a phase lag, even for disturbance frequencies close to the drift dynamics of the accelerometer. However, the influence of high-frequency noise is obviously much stronger as in the double integrator approach. The observer's frequency response is plotted in Fig. 10 and can be used to further investigate this undesirable property of the disturbance observer.

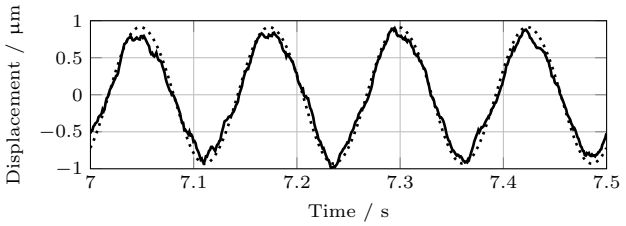

Fig. 9. Position estimated by the disturbance observer; solid: estimation $\hat{p}_\mathrm{d}$; dotted: strain gauge measurement p_d

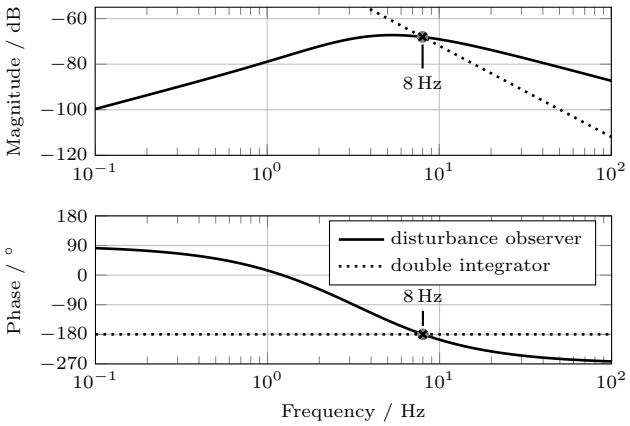

Fig. 10. Calculated Frequency Response of the disturbance observer: Acceleration measurement a to estimated position $\hat{p}_\mathrm{d}$

Just like the disturbance system itself, the observer is a third order system. In addition, the observer has to be a causal system with high-frequency roll-off to attenuate noise. This limits the number of zeros to two. As can be seen in the low-frequency slope with $+20\,^{\mathrm{dB}}/_{\mathrm{dec}}$ in Fig. 10, only one of the zeros is used for low-frequency attenuation. While one zero at the origin is sufficient to set the DC gain to zero, the attenuation of low-frequency drifts will be smaller than in the approach based on a double integrator, with both zeros at the origin and a $+40\,^{\mathrm{dB}}/_{\mathrm{dec}}$ low-frequency magnitude slope.

The second available zero is placed in the right half plane to induce phase lag, acting similar to an all-pass filter. This right half plane zero is obviously used to lower the phase and to match the phase exactly to -180 ° at the targeted frequency ω_0 solving the phase lead problem of the double integrator approach. Unlike an all-pass filter which could be added to the double integrator, a disturbance observer can also be designed to match both amplitude and phase for multiple disturbance frequencies.

Since the observer is a third order system with two zeros, the high-frequency magnitude slope is only $-20\,^{\mathrm{dB}}/_{\mathrm{dec}}$. This explains the poor attenuation of high frequency noise that is obvious in Fig. 9. The reconstructor based on double integration has a $-40\,^{\mathrm{dB}}/_{\mathrm{dec}}$ slope and thus better noise attenuation.

As a conclusion, a position reconstructor based on a disturbance observer solves the phase problem of the double integrator with filter approach, but has less attenuation for both low-frequency drifts and high-frequency noise. The double integrating behavior is matched perfectly at the disturbance frequency ω_0.

3.3 Adaptive Resonator

A novel position reconstruction approach for distinct disturbance frequencies, inspired by adaptive feedforward cancellation systems, Byl et al. [2005], is proposed to overcome these limitations. It will be shown that this reconstructor perfectly matches double integrating behavior at the targeted frequency ω_0 and attenuates both low- and high-frequency disturbances well.

The main idea is based on Fourier analysis of the disturbance input. Considering the nature of disturbance signals caused by structural resonances with distinct frequencies ω_0, the disturbance acceleration can be described by (6). The Fourier coefficients A and B therein are derived by Fourier analysis. This concept is used for online estimation by online Fourier analysis of the measured acceleration signal $a(t)$ that includes the actual disturbance acceleration, low-frequency drifts and offset as well as noise, as described in (7). The estimated Fourier coefficients are denoted by $\hat{A}$ and $\hat{B}$.

According to (6), a sinusoidal signal at the frequency ω_0 with the unknown amplitude values $\hat{A}$ and $\hat{B}$ is generated, Fig. 11. The difference of this estimated acceleration signal $\hat{\ddot{p}}_\mathrm{d}(t)$ and the measured acceleration signal $a(t)$, $\hat{\ddot{p}}_{\mathrm{d,err}}(t)$, is then analyzed by an online implementation of (7) which generates the estimates $\hat{A}$ and $\hat{B}$. The estimates of the Fourier coefficients are thus continuously updated, converging to the actual values A and B, Messner and Bodson [1995], Bayard [2000]. The rate of convergence increases with increasing loop gain g, Byl et al. [2005].

$$\ddot{p}_\mathrm{d}(t) = A\ \cos(\omega_0 t) + B\ \sin(\omega_0 t) \tag{6}$$

$$\hat{A}(t) = \int_{\tau=0}^{t} g\ \hat{\ddot{p}}_{\mathrm{d,err}}(\tau)\ \cos(\omega\tau)\ d\tau$$

$$\hat{B}(t) = \int_{\tau=0}^{t} g\ \hat{\ddot{p}}_{\mathrm{d,err}}(\tau)\ \sin(\omega\tau)\ d\tau \tag{7}$$

The reconstructor or observer based on this scheme, Fig. 11, can thus be regarded as a control loop with the measured acceleration as reference input and the estimated Fourier coefficients $\hat{A}$ and $\hat{B}$ as control efforts. The controlled plant is the signal generation according to (6) which is controlled such that the difference between the measured acceleration a and the estimated acceleration $\hat{\ddot{p}}_\mathrm{d}$ goes to zero at the disturbance frequency ω_0. The disturbance position is calculated from this estimate by multiplication with $^{-1}/_{\omega_0^2}$.

The reconstruction performance for the experiment with an 8 Hz, 0.8 µm sinusoid is depicted in Fig. 12. It is obvious that the position reconstruction is performed without any phase lag and that neither low-frequency drifts nor high-frequency disturbances affect the reconstructor output. Thus, the major drawbacks of reconstruction based on filtering and double integrating and based on a disturbance observer are not present in this reconstruction scheme.

It can be shown that the adaptive resonator system's input-output behavior is linear time-invariant, Messner and Bodson [1995], Bayard [2000]. This result is used

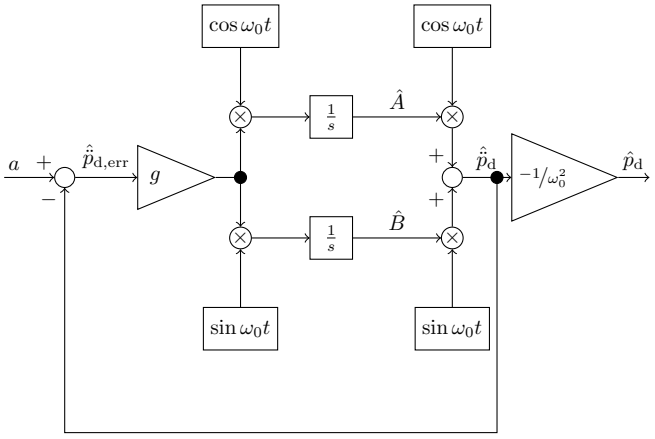

Fig. 11. Position reconstructor based on an adaptive resonator

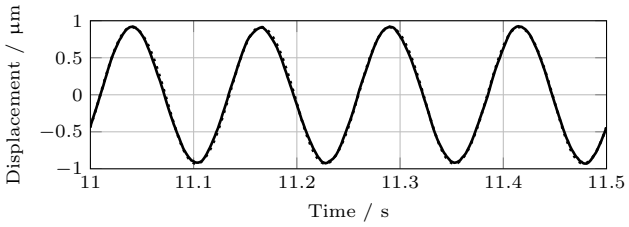

Fig. 12. Position estimated by the adaptive resonator reconstructor; solid: estimation $\hat{p}_\mathrm{d}$; dotted: strain gauge measurement p_d

for a further analysis of the reconstructor's properties, in particular the rejection of low-frequency drift and high-frequency noise. The frequency response of the overall reconstructor, (8) is plotted in Fig. 13.

$$H_\mathrm{adapt}(s) = \frac{\hat{p}_\mathrm{d}}{a}(s) = \frac{\frac{-g}{\omega_0^2}s}{s^2 + gs + \omega_0^2} \tag{8}$$

Since the targeted disturbance frequency ω_0 is located at the resonant peak of the system, the magnitude of the overall transfer function is kept comparably low. There is a distinct gain offset between desired and undesired frequency bands. Thus, low-frequency drifts at frequencies close to ω_0 can be attenuated well by keeping the resonant peak narrow enough to enforce low magnitude for the disturbances by retaining these frequencies to the $+20\,\mathrm{dB/dec}$ area outside the resonant peak.

Although the high-frequency slope is only -20 dB/dec, compared to -40 dB/dec in the case of a double integrator, the offset between the magnitude at ω_0 and in the adjacent areas decreases the magnitude for high frequencies as well. As can be seen in the experimental results, Fig. 12, this magnitude drop is sufficient to attenuate the influence of noise well. If problems with high-frequency noise arise, the reconstructor could simply be augmented by a low-pass filter. With increasing reconstructor loop gain g, the resonant peak becomes wider, increasing the magnitude in areas of undesired disturbance frequencies. Thus, the choice of g is a trade-off between convergence rate and disturbance rejection.

Summing up these considerations, the reconstruction approach based on an adaptive resonator permits position reconstruction without any phase lag by matching double integrating behaviour perfectly at the targeted frequency ω_0. Since the reconstructor transfer function has a resonant peak at this frequency, there is a fast magnitude drop between ω_0 and the areas of adjacent undesired disturbances. Several adaptive resonators can be placed in parallel in the reconstructor's feedback loop to match the resonant frequencies of the telescope structure.

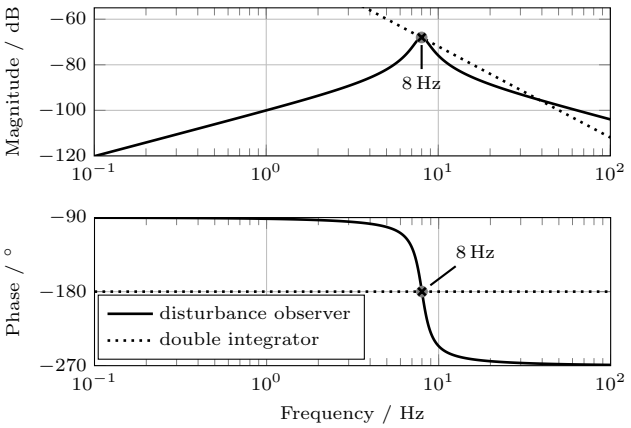

Fig. 13. Calculated Frequency Response of the adaptive resonator reconstructor: Acceleration measurement a to estimated position $\hat{p}_\mathrm{d}$

4. CONCLUSION

Three different approaches for reconstruction of disturbance position from accelerometer measurements have been analyzed and evaluated in laboratory. The considered application, the reconstruction of disturbances due to structural vibrations in telescopes, demands high reconstruction accuracy and good attenuation of both low-frequency drifts and high-frequency noise in the measurement chain.

The first approach, double integration and filtering, attenuates noise well but large filter corner frequencies for drift suppression induce substantial phase lag in the position signal for small disturbance frequencies. A disturbance observer was designed to overcome this problem. However, due to the observer's structure, the noise attenuation turned out to be worse. Thus, a novel position reconstruction approach based on adaptive resonators was investigated. A reconstructor based on this scheme permits highly accurate position reconstruction as well as good attenuation of both low-frequency drifts and high-frequency noise.

As a next step, the reconstruction of disturbance vibrations with several distinct resonant frequencies and the overall performance of position reconstruction and correction with an additional tip-tilt mirror as correction unit will be investigated.

ACKNOWLEDGEMENTS

The authors would like to thank the German Federal Ministry of Education and Research (BMBF) for supporting this work as well as the colleagues at ISYS and MPIA, especially Michael Böhm and Diethard Peter for their helpful suggestions and comments.

REFERENCES

D. S. Bayard. A general theory of linear time-invariant adaptive feedforward systems with harmonic regressors. *IEEE Transactions on Automatic Control*, 45: 1983–1996, 2000.

M. Böhm, J.-U. Pott, M. Kürster, and O. Sawodny. Modeling and identification of the optical path at ELTs - a case study at the LBT. *Proc. of the 6th IFAC Symposium on Mechatronic Systems*, 6:249–255, April 2013.

M. F. Byl, S. J. Ludwick, and D. L. Trumper. A loop shaping perspective for tuning controllers with adaptive feedforward cancellation. *Precision Engineering*, 29:27–40, 2005.

G. F. Franklin, J. D. Powell, and M. L. Workman. *Digital control of dynamic systems*. Addison-Wesley, 1997.

J.-M. Godhavn. Adaptive tuning of heave filter in motion sensor. In *OCEANS 98 Conference Proceedings*, volume 1, pages 174–178, 1998.

J. W. Hardy. *Adaptive optics for astronomical telescopes*. Oxford Univ. Press, New York, 1998.

M. Kürster, T. Bertram, J. L. Borelli, M. Brix, W. Gässler, T. M. Herbst, V. Naranjo, J.-U. Pott, J. Trowitzsch, T. E. Connors, P. M. Hinz, T. J. McMahon, D. S. Ashby, J. G. Brynnel, N. J. Cushing, T. Edgin, J. D. Esguerra, R. F. Green, J. Kraus, J. Little, U. Beckmann, and G. P. Weigelt. OVMS: the optical path difference and vibration monitoring system for the LBT and its interferometers. In *Society of Photo-Optical Instrumentation Engineers (SPIE) Conference Series*, volume 7734, 2010.

W. Messner and M. Bodson. Design of adaptive feedforward algorithms using internal model equivalence. *International Journal of Adaptive Control and Signal Processing*, 9:199–212, 1995.

T. Ruppel, S. Dong, F. Rooms, W. Osten, and O. Sawodny. Feedforward control of deformable membrane mirrors for adaptive optics. *IEEE Transactions on Control Systems Technology*, 3:579–589, 2013.

A. H. Slocum. *Precision machine design*. Prentice-Hall, 1992.